Available online at www.sciencedirect.com
SCIENCE DIRECT®
Journal of Organometallic Chemistry 669 (2003) 124–134
Journal of Organometallic Chemistry
www.elsevier.com/locate/jorganchem

Syntheses of a series of trinuclear MIr_2 or pentanuclear MIr_4 bimetallic bis(selenido) and selenido–sulfido clusters (M = Pd, Pt, Fe, Co) from diiridium μ-bis(hydroselenido) and μ-hydroselenido–hydrosulfido complexes $[\{(\eta^5\text{-}C_5Me_5)IrCl\}_2(\mu\text{-}SeH)(\mu\text{-}EH)]$ (E = Se, S)

Shoken Nagao [a], Hidetake Seino [a], Masanobu Hidai [b], Yasushi Mizobe [a,*]

[a] *Institute of Industrial Science, The University of Tokyo, Komaba, Meguro-ku, Tokyo 153-8505, Japan*
[b] *Department of Materials Science and Technology, Faculty of Industrial Science and Technology, Tokyo University of Science, Noda, Chiba 278-8510, Japan*

Received 25 November 2002; received in revised form 10 December 2002; accepted 26 December 2002

Abstract

Reactions of a diiridium μ-bis(hydroselenido) complex $[Cp^*IrCl(\mu\text{-}SeH)_2IrCp^*Cl]$ (**1a**; $Cp^* = \eta^5\text{-}C_5Me_5$) with $[MCl_2(cod)]$ (M = Pd, Pt; cod = 1,5-cyclooctadiene), $FeCl_2$, and $CoCl_2$ readily afforded the bimetallic selenido clusters containing a trinuclear or a pentanuclear cores $[(Cp^*Ir)_2(MCl_2)(\mu_3\text{-}Se)_2]$ (M = Pd, Pt (**5**), Fe (**6**)) and $[(Cp^*Ir)_4Co(\mu_3\text{-}Se)_4][CoCl_3(MeCN)]_2$ (**8**). Cluster **6** was converted to the latter-type bow-tie cluster $[(Cp^*Ir)_4Fe(\mu_3\text{-}Se)_4][BPh_4]_2$ (**7**) by treatment with an additional amount of **1a** and excess $NaBPh_4$. Novel μ-hydroselenido–hydrosulfido complex $[Cp^*IrCl(\mu\text{-}SeH)(\mu\text{-}SH)IrCp^*Cl]$ (**3**) was obtained by the reaction of $[Cp^*IrCl(\mu\text{-}Cl)_2IrCp^*Cl]$ with one equiv of H_2Se generated in situ from a NaSeH/HCl aq. mixture, followed by that with H_2S gas. Treatment of **3** with a range of transition metal compounds has shown that **3** can serve as a good precursor to synthesize a series of mixed-chalcogenido clusters in a rational manner; selenido–sulfido clusters derived from **3** include $[(Cp^*Ir)_2(MCl_2)(\mu_3\text{-}Se)(\mu_3\text{-}S)]$ (M = Pd, Pt, Fe (**14**)), $[(Cp^*Ir)_2\{PtCl(PPh_3)\}(\mu_3\text{-}Se)(\mu_3\text{-}S)]Cl$ (**13**), $[(Cp^*Ir)_4Co(\mu_3\text{-}Se)_2(\mu_3\text{-}S)_2][CoCl_3(MeCN)]_2$ (**15**), and $[(Cp^*Ir)_4Fe(\mu_3\text{-}Se)_2(\mu_3\text{-}S)_2][BPh_4]_2$. To determine the detailed structures, X-ray analyses have been undertaken for **5**·1/2$ClCH_2CH_2Cl$, **6**, **7**, **8**, **13**·CH_2Cl_2, **14**, and **15**·CH_2Cl_2.

Keywords: Bimetallic selenido clusters; Trinuclear and pentanuclear cores; Diiridium hydroselenido complexes

1. Introduction

Our extensive studies on the exploration of the rational routes leading to the high-yield synthesis of homo- and hetero-metallic sulfido clusters with desired core structures and atom compositions [1] have recently been extended to those of the corresponding selenido clusters. Thus, we have reported the syntheses of a diiridium μ-tetraselenido complex $[Cp^*Ir(\mu\text{-}Se_4)_2IrCp^*]$ ($Cp^* = \eta^5\text{-}C_5Me_5$) [2] along with dinuclear μ-hydroselenido complexes such as $[Cp^*MCl(\mu\text{-}SeH)_2MCp^*Cl]$ (M = Ir (**1a**), M = Rh (**1b**)) [3] and $[CymRuCl(\mu\text{-}SeH)_2RuCymCl]$ (Cym = *p*-cymene) [4], and these dinuclear complexes have proved to serve as good precursors to a range of new homo- and hetero-metallic

* Corresponding author. Tel.: +81-3-5452-6360; fax: +81-3-5452-6361.
E-mail address: ymizobe@iis.u-tokyo.ac.jp (Y. Mizobe).

0022-328X/03/$ - see front matter © 2003 Elsevier Science B.V. All rights reserved.
doi:10.1016/S0022-328X(02)02226-X

clusters with μ-selenido ligands. These include the $Ir_2Pd_2Se_3$ and $Ir_2Pd_3Se_5$ clusters obtained from the former iridium tetraselenido complex [2a] and the cubane-type M_4Se_4 clusters (M = Ir, Rh, Ru) derived from the latter hydroselenido complexes [3,4].

Since our previous studies have already shown that the μ-hydrosulfido complexes [Cp*MCl(μ-SH)$_2$-MCp*Cl] (**2**; M = Ru, Ir, Rh) are quite versatile for preparing not only the cubane-type tetranuclear clusters but also numerous trinuclear and pentanuclear sulfido clusters [5], conversion of **1a**, which is the selenium analogue of **2a** (M = Ir), into the bimetallic selenido clusters with triangular cores or pentanuclear bow-tie cores has been investigated in this study. Furthermore, we have succeeded in preparing a new diiridium complex having both the hydroselenido and hydrosulfido ligands [Cp*IrCl(μ-SeH)(μ-SH)IrCp*Cl] (**3**), which has proved to be an excellent starting complex to obtain the mixed-chalcogenido clusters containing both the selenido and sulfido ligands. This represents one of the still rare pathways leading to the formation of tailored mixed-chalcogenido clusters and its details are also reported herein.

2. Results and discussion

2.1. Reactions of *1a* with transition metal compounds

As reported already, [Cp*MCl(μ-SH)$_2$MCp*Cl] (M = Ir (**2a**), Rh (**2b**), Ru (**2c**)) readily react with various metal compounds accompanied by dehydrochlorination to give a trinuclear clusters with two capping sulfido ligands, which are formulated as $[(Cp^*M)_2(M'L_m)(\mu_3\text{-}S)_2]^n$ (e.g. M = Ir: $M'L_m$ = $PdCl_2$, $PdCl(PPh_3)$ [5a], $RuCl_2(PPh_3)$; M = Ir, Rh: $M'L_m$ = Rh(cod) (cod = 1,5-cyclooctadiene) [5c], $FeCl_2$ [5d]; M = Ru: $M'L_m$ = $RuCl(PPh_3)_2(\mu\text{-H})$ [5e], $RhCl_2(PPh_3)(\mu\text{-H})$ [5f]; etc.). In the preceding paper [3], we described the syntheses of the Ir and Rh μ-hydroselenido analogues **1** and the subsequent transformations of the Rh complex **1b** into triangular $Rh_3(\mu_3\text{-}Se)_2$ clusters such as $[(Cp^*Rh)_2(RhL_2)(\mu_3\text{-}Se)_2]^+$ (L = CO, PPh_3) and $[(Cp^*Rh)_3(\mu_3\text{-}Se)_2]^{2+}$ along with the condensation of two molecules of **1** to afford the cubane-type tetranuclear clusters $[(Cp^*M)_4(\mu_3\text{-}Se)_4]$ (M = Ir, Rh).

Now it has been found that the reactions of **1a** with one equiv of $[PdCl_2(cod)]$ or $[PtCl_2(cod)]$ in THF proceed in an analogous manner to those of **2a** to give the trinuclear bimetallic selenido clusters $[(Cp^*Ir)_2(MCl_2)(\mu_3\text{-}Se)_2]$ (M = Pd (**4**), Pt (**5**)) as green crystals (Eq. (1)).

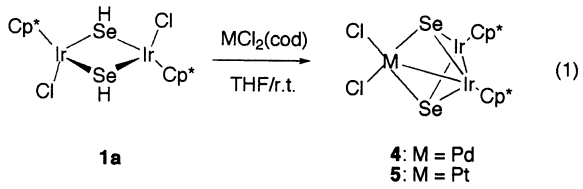

1a **4**: M = Pd **5**: M = Pt (1)

It is noteworthy that the reactions occur more smoothly for **1a** as compared to those of the hydrosulfido analogue **2a**. Thus, the reactions of **1a** yielding **4** and **5** complete in several hours at room temperature, whereas to convert all **2a** cleanly into the corresponding sulfido clusters higher reaction temperatures (e.g. 50 °C) were required. Single-crystal X-ray analysis has been carried out for **5** to confirm the structures of these products, the results of which are shown in Fig. 1.

The reaction of **1a** with an equimolar amount of $FeCl_2$ in THF at room temperature also gave a trinuclear selenido cluster $[(Cp^*Ir)_2(FeCl_2)(\mu_3\text{-}Se)_2]$ (**6**) as black crystals (Scheme 1). Subsequent treatment of paramagnetic **6** with one equiv of **1a** in the presence of $NaBPh_4$ in THF at room temperature resulted in the formation of the diamagnetic pentanuclear complex with a bow-tie core $[(Cp^*Ir)_4Fe(\mu_3\text{-}Se)_4][BPh_4]_2$ (**7**) as red crystals (Scheme 1). Cluster **7** was also obtained by reacting **6** with only $NaBPh_4$, presumably via the degradation of the Ir_2Fe core of part of **6**. Both **6** and **7** have been fully characterized by the X-ray analyses, whose structures are depicted in Figs. 2 and 3, respectively. Analogous reactions of **1a** were also carried out with $CoCl_2$ and $NiCl_2$, which showed that only the pentanuclear cluster $[(Cp^*Ir)_4Co(\mu_3\text{-}Se)_4][CoCl_3(MeCN)]_2$ (**8**) was isolable by treatment with the former, the product(s) from **1a** and $NiCl_2$ being intractable. Although the reaction of equimolar amounts of **1a** and

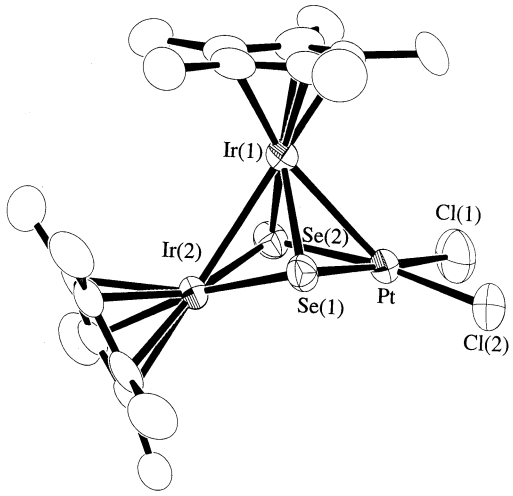

Fig. 1. An ORTEP drawing of **5**. Thermal ellipsoids are drawn at the 50% probability level. Hydrogen atoms and solvating $ClCH_2CH_2Cl$ are omitted for clarity.

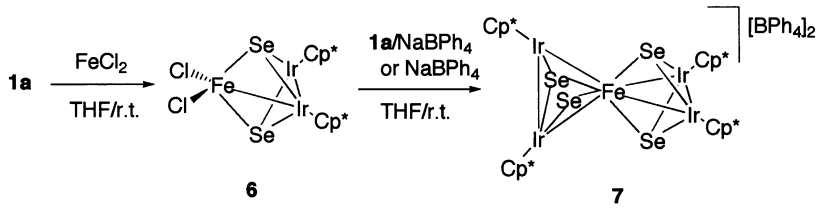

Scheme 1.

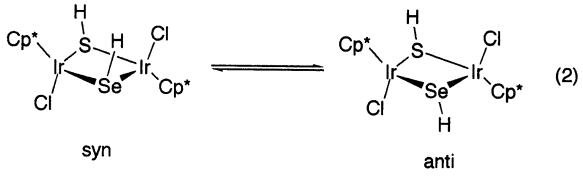

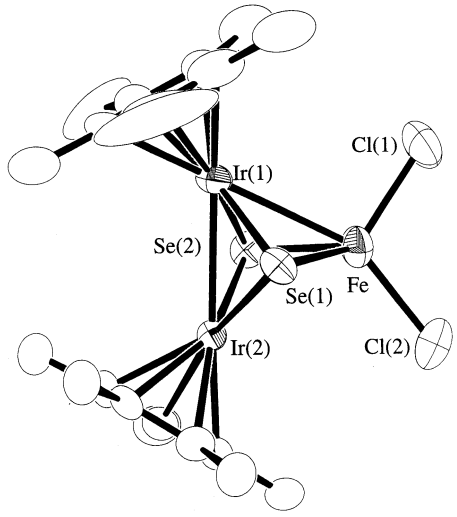

Fig. 2. An ORTEP drawing of **6**. Thermal ellipsoids are drawn at the 50% probability level. Hydrogen atoms are omitted for clarity.

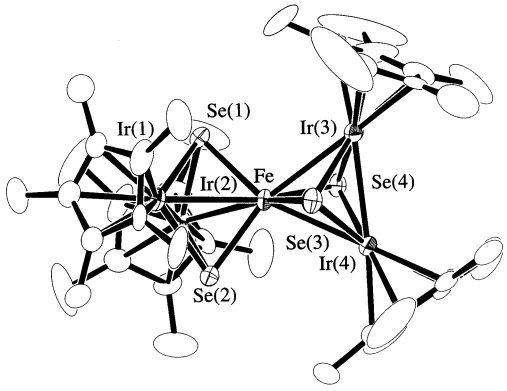

Fig. 3. An ORTEP drawing of **7**. Thermal ellipsoids are drawn at the 30% probability level. The anions and hydrogen atoms are omitted for clarity.

$CoCl_2$ directly gave **8**, the yield was quite low. However, when treated with 1.5 equivalents of $CoCl_2$ as required from the Co:Ir ratio of 3:4 in **8**, **1a** was converted into **8** in satisfactory yield. These results on the reactions of **1a** with $FeCl_2$ and $CoCl_2$ are analogous to those of the hydrosulfido complex **2a** previously observed [5d]. By contrast, although the $NiIr_4$ sulfido cluster was also available from **2a** and $NiCl_2$ under more forcing condtions, somehow the corresponding Se cluster could not be obtained from the reactions using **1a**. Cluster **8** has been characterized by the X-ray analysis as depicted in Fig. 4.

2.2. Synthesis of diiridium μ-hydroselenido–hydrosulfido complex *3*

Since the diiridium complexes with two bridging hydrochalcogenido ligands **1a** and **2a** have turned out to be quite excellent precursors to synthesize a variety of chalcogenido clusters, attempts have been made to prepare a diiridium mixed-hydrochalcogenido complex, aiming at derivatizing mixed-chalcogenido clusters in a rational manner.

Now we have found that when [Cp*IrCl(μ-$Cl)_2$IrCp*Cl] (**9**) was treated with one equiv of H_2Se, which was generated in situ from one equiv of NaSeH and 1.15 equivalents of HCl aq. in CH_2Cl_2 at 0 °C, a μ-hydoselenido complex [Cp*IrCl(μ-SeH)(μ-Cl)IrCp*Cl] (**10**) was obtained as a major product (Scheme 2). Thus, the ^{1}H-NMR spectrum of the reaction mixture

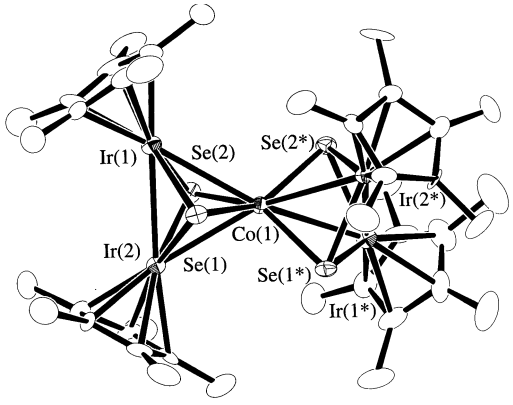

Fig. 4. An ORTEP drawing of **8**. Thermal ellipsoids are drawn at the 30% probability level. The anions and hydrogen atoms are omitted for clarity.

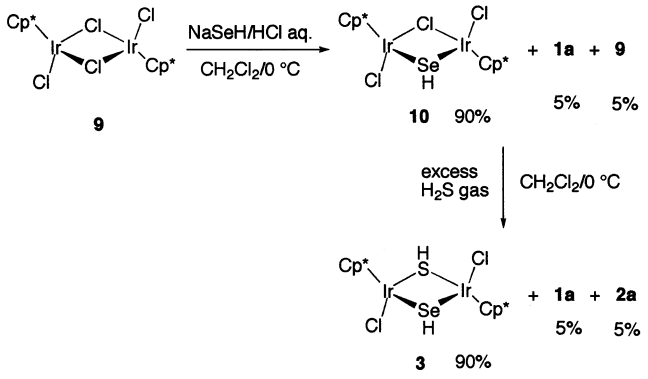

Scheme 2.

showed the presence of **10**, bis(hydroselenido) complex **1a**, and the unreacted **9** in a ratio of 18:1:1, indicating clearly that the initial replacement of the Cl ligand in **9** forming **10** is much faster than the following substitution reaction converting **10** into **1a** at room temperature. By contrast, treatment of **9** under similar conditions with one equiv of H_2S generated analogously from NaSH and HCl aq. has resulted in the formation of a mixture containing [Cp*IrCl(μ-SH)(μ-Cl)IrCp*Cl], bis(hydrosulfido) complex **2a**, and the unreacted **9** in a ratio of 2:1:1.

Since the isolation of **10** in pure form was unsuccessful, the resultant reaction mixture containing **10** as the major component was successively treated with an excess of H_2S gas at 0 °C, which afforded a mixture containing the desired mixed-hydrochalcogenido complex **3** (90%) along with impurities **1a** (5%) and **2a** (5%) (Scheme 2). This result indicates that the replacement of the μ-SeH ligand by the SH anion does not take place under these conditions. Attempts to isolate analytically pure **3** were unsuccessful, the following syntheses of the mixed chalcogenido clusters were conducted by the use of this product without further purification.

As observed previously for the precedented μ-hydroselenido and μ-hydrosulfido complexes **1** and **2**, the ^{1}H-NMR spectrum showed that **3** exists as a mixture of *syn* and *anti* forms with respect to the two μ-EH (E = S, Se) groups in solution (Eq. (2)).Thus, previous work has shown that both **1a** and **2a** are present in C_6D_6 at room temperature as a mixture of the *syn* and *anti* forms in a ratio of 3:2, which was easily determined on the basis of the intensity ratio of the Cp* resonances assignable to these two isomers: two singlets with the same intensities for the *syn* isomers and one singlet for the *anti* isomers. By contrast, for **3** both the *syn* and *anti* forms contain two inequivalent Cp* groups and show two Cp* resonances. Hence, the signals due to the two isomers are unable to be assigned unambiguously. However, also for the hydroselenido–hydrosulfido complex **3**, two sets of the Cp* signals appeared in an intensity ratio of 3:2 as observed for the bis(hydroselenido) complex **1a** and the bis(hydrosulfido) complex **2a**. Furthermore, the difference in the chemical shifts of the two Cp* singlets due to the predominant isomer of **3** (0.21 ppm), which is much larger than that of the minor isomer (0.04 ppm), is in good agreement with those observed for the *syn* isomers of both **1a** (0.19 ppm) [3] and **2a** (0.23 ppm) [5c,6]. These data might suggest that the predominant form in solution might be assignable to be syn also for **3**.

2.3. Syntheses of mixed-metal mixed-chalcogenido clusters

Reactions of **3** with a range of transition metal compounds were carried out in an analogous manner to those of **1a**. Thus, when **3** was allowed to react with one equiv of [MCl_2(cod)] (M = Pd, Pt), expected selenido–sulfido clusters [(Cp*Ir)$_2$(MCl_2)(μ$_3$-Se)(μ$_3$-S)] (M = Pd (**11**), Pt (**12**)) were obtained as green crystals in moderate yields. Cluster **12** was further reacted with an equimolar amount of PPh_3 to afford a cationic cluster [(Cp*Ir)$_2${PtCl(PPh_3)}(μ$_3$-Se)(μ$_3$-S)]Cl (**13**) (Scheme 3), whose structure was determined unequivocally by the X-ray analysis (Fig. 5). Despite the use of a starting complex **3** contaminated with **1a** and **2a**, these products are pure from the ^{1}H-NMR criteria and the elemental analyses also gave the satisfactory results.

Complex **3** also reacted with $FeCl_2$ and $CoCl_2$ under the conditions essentially analogous to those for preparing **6** and **8** from **1a**, yielding paramagnetic [(Cp*Ir)$_2$($FeCl_2$)(μ$_3$-Se)(μ$_3$-S)] (**14**) and [(Cp*Ir)$_4$Co(μ$_3$-Se)$_2$(μ$_3$-S)$_2$][$CoCl_3$(MeCN)]$_2$ (**15**), respectively. The former was convertible to an expected diamagnetic bow-tie

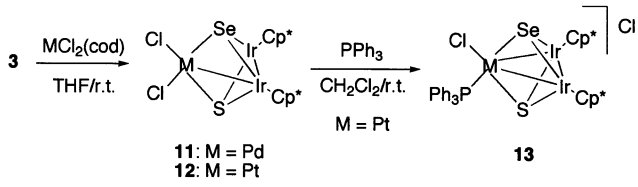

Scheme 3.

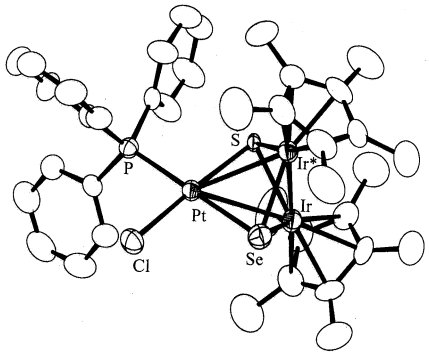

Fig. 5. An ORTEP drawing of **13**. Thermal ellipsoids are drawn at the 50% probability level. Hydrogen atoms and solvating CH_2Cl_2 are omitted for clarity.

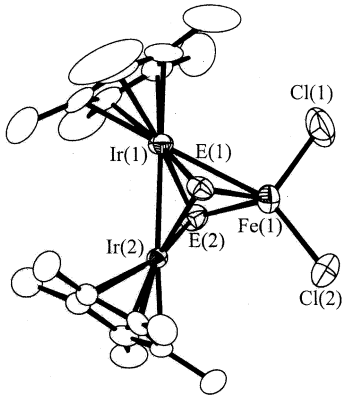

Fig. 6. An ORTEP drawing of **14**. Thermal ellipsoids are drawn at the 50% probability level. Hydrogen atoms are omitted for clarity.

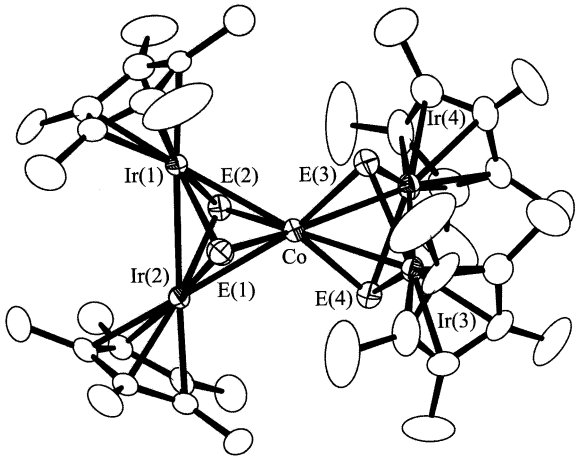

Fig. 7. An ORTEP drawing of **15**. Thermal ellipsoids are drawn at the 30% probability level. The anions and hydrogen atoms along with solvating CH_2Cl_2 are omitted for clarity.

cluster $[(Cp^*Ir)_4Fe(\mu_3\text{-}Se)_2(\mu_3\text{-}S)_2][BPh_4]_2$ (**16**) similarly (Scheme 4). In the FAB-MS spectrum of **14**, the peak assignable to the ion $[\mathbf{14}-Cl]^+$ appeared, whereby those arising from the bis(selenido) and bis(sulfido) analogues of **14** were not detectable. This also indicates that only the selenido–sulfido cluster **14** was isolated in a pure form. Clusters **14** and **15** have been characterized by the X-ray diffraction as shown in Figs. 6 and 7.

Reactivities displayed at the multinuclear metal–sulfido sites and their selenido analogues are currently attracting increasing interest in relevance to certain biological and industrial catalysis, and the mixed-chalcogenido clusters are of considerable importance because of their potential as good models to clarify the site selectivity exhibited at the multimetallic mixed-chalcogenido site. However, although a range of sulfido–selenido, sulfido–telurido, and selenido–telurido clusters are known, which include, for example, those derived from $[Fe_2(\mu\text{-}EE')(CO)_6]$ (E, E′ = S, Se, Te) [7], well-defined mixed-chalcogenido clusters are still rare and little is known about the methods to prepare such clusters in a reliable manner [8]. The reactions using the μ-hydroselenido–hydrosulfido complex **3** reported here may therefore represent quite a powerful method to obtain mixed selenido–sulfido clusters numerously. Reactivities of new selenido–sulfido clusters are now under investigation and the results will be described elsewhere.

2.4. Description of the X-ray structures of bis(selenido) and selenido–sulfido clusters

The X-ray analyses have been carried out to determine the detailed structures for diselenido clusters **5**, **6**, **7** and **8** as well as selenido–sulfido clusters **13**, **14** and **15**. Pertinent bonding parameters in these clusters are listed in Tables 1–7, respectively.

As shown in Fig. 1, **5** has a triangular core, for which the Ir–Ir distance at 2.913(1) Å and one Pt–Ir distance at 2.751(1) Å fall in the range of the metal–metal single bond lengths, whereas the remaining Pt–Ir distance is

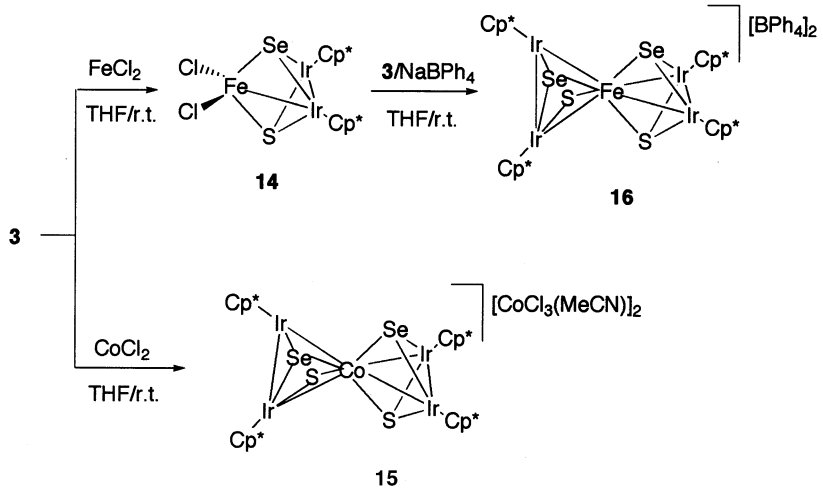

Scheme 4.

Table 1
Selected bond lengths (Å) and bond angles (°) in **5**

Bond lengths			
Pt–Ir(1)	2.751(1)	Pt···Ir(2)	3.487(1)
Ir(1)–Ir(2)	2.913(1)	Pt–Se(2)	2.411(2)
Pt–Se(1)	2.408(2)	Pt–Cl(2)	2.366(5)
Pt–Cl(1)	2.352(5)	Ir(1)–Se(2)	2.424(2)
Ir(1)–Se(1)	2.435(2)	Ir(2)–Se(2)	2.410(2)
Ir(2)–Se(1)	2.413(2)		
Bond angles			
Pt–Ir(1)–Ir(2)	75.94(3)	Se(1)–Pt–Cl(1)	175.1(2)
Se(1)–Pt–Se(2)	83.99(7)	Se(2)–Pt–Cl(1)	91.1(2)
Se(1)–Pt–Cl(2)	92.5(1)	Cl(1)–Pt–Cl(2)	92.4(2)
Se(2)–Pt–Cl(2)	172.6(2)	Se(1)–Ir(2)–Se(2)	83.88(7)
Se(1)–Ir(1)–Se(2)	83.12(6)	Pt–Se(1)–Ir(2)	92.64(7)
Pt–Se(1)–Ir(1)	69.21(5)	Pt–Se(2)–Ir(1)	69.36(5)
Ir(1)–Se(1)–Ir(2)	73.84(5)	Ir(1)–Se(2)–Ir(2)	74.09(5)
Pt–Se(2)–Ir(2)	92.65(7)		

Table 2
Selected bond lengths (Å) and bond angles (°) in **6**

Bond lengths			
Fe–Ir(1)	2.926(2)	Fe···Ir(2)	3.120(2)
Ir(1)–Ir(2)	2.8520(6)	Fe–Se(2)	2.444(2)
Fe–Se(1)	2.455(2)	Fe–Cl(2)	2.252(4)
Fe–Cl(1)	2.230(5)	Ir(1)–Se(2)	2.422(1)
Ir(1)–Se(1)	2.425(1)	Ir(2)–Se(2)	2.413(1)
Ir(2)–Se(1)	2.415(1)		
Bond angles			
Fe–Ir(1)–Ir(2)	65.35(4)	Se(1)–Fe–Cl(1)	120.1(2)
Se(1)–Fe–Se(2)	89.14(6)	Se(2)–Fe–Cl(1)	114.2(1)
Se(1)–Fe–Cl(2)	110.4(1)	Cl(1)–Fe–Cl(2)	107.9(2)
Se(2)–Fe–Cl(2)	114.6(1)	Se(1)–Ir(2)–Se(2)	90.84(4)
Se(1)–Ir(1)–Se(2)	90.39(4)	Fe–Se(1)–Ir(2)	79.68(5)
Fe–Se(1)–Ir(1)	73.68(5)	Fe–Se(2)–Ir(1)	73.92(5)
Ir(1)–Se(1)–Ir(2)	72.22(4)	Ir(1)–Se(2)–Ir(2)	72.30(3)
Fe–Se(2)–Ir(2)	79.92(6)		

elongated to a non-bonding one at 3.487(1) Å. Thus, the $PtIr_2Se_2$ core has rather a square pyramidal structure with the Ir(1) atom at the apex than a trigonal bipyramid with two apical Se atoms. Analogous square pyramidal cores have been demonstrated for the M_3Se_2 clusters of e.g. M = Fe, Ru [9]. Inequivalency was also observed for the two Fe–Ir distances in **6** (2.926(2) and 3.120(2) Å) but apparently the difference is much smaller than that in **5**, and the geometry of the $FeIr_2Se_2$ core in **6** is close to a trigonal bypyramid as depicted in Fig. 2. It is also noteworthy that both of the two Fe–Ir bonds are longer than the Ir–Ir bond at 2.8520(6) Å, indicating the weaker interactions present between Fe and Ir atoms. In the related sulfido cluster $[(Cp^*Ir)_2(FeCl)_2(\mu_3\text{-}S)_2]$ (**17**) [5d], the Fe–Ir distances are 2.880(3) and 3.006(3) Å, displaying the comparable inequivalency but both being slightly shorter than those in the selenido cluster **6**.

Table 3
Selected bond lengths (Å) and bond angles (°) in **7**

Bond lengths			
Fe–Ir(1)	2.742(2)	Fe–Ir(2)	2.759(3)
Fe–Ir(3)	2.770(3)	Fe–Ir(4)	2.758(2)
Ir(1)–Ir(2)	2.8121(9)	Ir(3)–Ir(4)	2.799(1)
Fe–Se(1)	2.279(3)	Fe–Se(2)	2.282(3)
Fe–Se(3)	2.280(3)	Fe–Se(4)	2.274(3)
Ir(1)–Se(1)	2.394(2)	Ir(1)–Se(2)	2.395(2)
Ir(2)–Se(1)	2.393(2)	Ir(2)–Se(2)	2.398(2)
Ir(3)–Se(3)	2.394(2)	Ir(3)–Se(4)	2.403(2)
Ir(4)–Se(3)	2.404(2)	Ir(4)–Se(4)	2.383(2)
Bond angles			
Ir(1)–Fe–Ir(2)	61.49(5)	Fe–Ir(1)–Ir(2)	59.57(5)
Fe–Ir(2)–Ir(1)	58.95(5)	Se(1)–Fe–Se(2)	98.6(1)
Se(1)–Fe–Se(3)	127.2(1)	Se(1)–Fe–Se(4)	104.2(1)
Se(2)–Fe–Se(3)	105.0(1)	Se(2)–Fe–Se(4)	126.3(1)
Se(3)–Fe–Se(4)	98.5(1)	Se(1)–Ir(1)–Se(2)	92.46(6)
Se(1)–Ir(2)–Se(2)	92.41(7)	Se(3)–Ir(3)–Se(4)	92.01(7)
Se(3)–Ir(4)–Se(4)	92.25(7)	Fe–Se(1)–Ir(1)	71.80(8)
Fe–Se(1)–Ir(2)	72.36(8)	Ir(1)–Se(1)–Ir(2)	71.95(6)
Fe–Se(2)–Ir(1)	71.72(8)	Fe–Se(2)–Ir(2)	72.21(8)
Ir(1)–Se(2)–Ir(2)	71.84(5)	Fe–Se(3)–Ir(3)	72.64(8)
Fe–Se(3)–Ir(4)	72.10(8)	Ir(3)–Se(3)–Ir(4)	71.37(5)
Fe–Se(4)–Ir(3)	72.56(8)	Fe–Se(4)–Ir(4)	72.57(8)
Ir(3)–Se(4)–Ir(4)	71.56(5)		

Table 4
Selected bond lengths (Å) and bond angles (°) in **8**

Bond lengths			
Co(1)–Ir(1)	2.913(1)	Co(1)–Ir(2)	2.804(1)
Ir(1)–Ir(2)	2.873(1)	Co(1)–Se(2)	2.293(3)
Co(1)–Se(1)	2.302(3)	Ir(1)–Se(2)	2.422(2)
Ir(1)–Se(1)	2.395(2)	Ir(2)–Se(2)	2.397(2)
Ir(2)–Se(1)	2.415(2)		
Bond angles			
Ir(1)–Co(1)–Ir(2)	60.30(2)	Co(1)–Ir(1)–Ir(2)	57.96(4)
Co(1)–Ir(2)–Ir(1)	61.74(4)	Se(1)–Co(1)–Se(1*)	95.7(2)
Se(1)–Co(1)–Se(2)	95.19(8)	Se(2)–Co(1)–Se(2*)	96.4(2)
Se(1)–Co(1)–Se(2*)	143.48(7)	Se(1)–Ir(2)–Se(2)	89.66(7)
Se(1)–Ir(1)–Se(2)	89.55(7)	Co(1)–Se(1)–Ir(2)	72.90(6)
Co(1)–Se(1)–Ir(1)	76.65(8)	Co(1)–Se(2)–Ir(1)	76.27(6)
Ir(1)–Se(1)–Ir(2)	73.36(6)	Ir(1)–Se(2)–Ir(2)	73.19(6)
Co(1)–Se(2)–Ir(2)	73.38(8)		

The Ir–Se bond lengths in **5** and **6** are essentailly the same (2.410(2)–2.435(2) Å), which are longer than the Ir–S bond distances in **17** (2.280(5)–2.328(6) Å) as expected from the difference in the single-bond covalent radius of Se at 1.17 Å and that of S at 1.04 Å [10]. For comparison, the Ir(III)–Se distances in the selenido clusters reported previously are, e.g. 2.402(1)–2.409(2) Å in $[(Cp^*Ir)_3(\mu_3\text{-}Se)_2][PF_6]_2$ [3] and 2.482(2)–2.501(2) Å in $[(Cp^*Ir)_4(\mu_3\text{-}Se)_4]$ [11]. The Pt in **5** and the Fe in **6** are each bonded to two Cl anions, and if the metal–metal bonds are ignored, the geometry around the Pt is essentially square planar, while that around the Fe is almost tetrahedral. The Pt–Se bond lengths in **5** are 2.408(2) and 2.411(2) Å, which are shorter than the Fe–

Table 5
Selected bond lengths (Å) and bond angles (°) in **13**

Bond lengths			
Pt–Ir	3.041(1)	Ir–Ir*	2.935(1)
Pt–Se	2.470(1)	Pt–S	2.350(2)
Pt–Cl	2.351(3)	Pt–P	2.262(3)
Ir–S	2.347(2)		
Bond angles			
Ir–Pt–Ir*	57.71(2)	Pt–Ir–Ir*	61.15(1)
Se–Pt–S	85.99(7)	Se–Pt–Cl	90.63(9)
Se–Pt–P	179.40(9)	S–Pt–Cl	176.6(1)
S–Pt–P	93.41(9)	Cl–Pt–P	90.0(1)
Se–Ir–S	87.30(5)	Ir–Se–Ir*	74.80(4)
Pt–Se–Ir	76.97(4)	Ir–S–Ir*	77.40(7)
Pt–S–Ir	80.70(7)		

Table 6
Selected bond lengths (Å) and bond angles (°) in **14**

Bond lengths			
Fe–Ir(1)	2.898(1)	Fe···Ir(2)	3.056(1)
Ir(1)–Ir(2)	2.826(1)	Fe–E(2)	2.398(2)
Fe–E(1)	2.414(2)	Fe–Cl(2)	2.251(3)
Fe–Cl(1)	2.227(3)	Ir(1)–E(2)	2.376(1)
Ir(1)–E(1)	2.399(1)	Ir(2)–E(2)	2.364(1)
Ir(2)–E(1)	2.386(1)		
Bond angles			
Fe–Ir(1)–Ir(2)	64.52(4)	E(1)–Fe–Cl(1)	120.0(1)
E(1)–Fe–E(2)	89.05(6)	E(2)–Fe–Cl(1)	113.3(1)
E(1)–Fe–Cl(2)	110.69(9)	Cl(1)–Fe–Cl(2)	107.6(1)
E(2)–Fe–Cl(2)	115.63(9)	E(1)–Ir(2)–E(2)	90.52(4)
E(1)–Ir(1)–E(2)	89.90(4)	Fe–E(1)–Ir(2)	79.09(5)
Fe–E(1)–Ir(1)	74.03(4)	Fe–E(2)–Ir(1)	74.75(5)
Ir(1)–E(1)–Ir(2)	72.40(4)	Ir(1)–E(2)–Ir(2)	73.19(4)
Fe–E(2)–Ir(2)	79.84(5)		

Table 7
Selected bond lengths (Å) and bond angles (°) in **15**

Bond lengths			
Co(1)–Ir(1)	2.796(2)	Co(1)–Ir(2)	2.755(2)
Co(1)–Ir(3)	2.803(2)	Co(1)–Ir(4)	2.773(2)
Ir(1)–Ir(2)	2.840(1)	Ir(3)–Ir(4)	2.825(1)
Co(1)–E(1)	2.274(2)	Co(1)–E(2)	2.287(2)
Co(1)–E(3)	2.275(2)	Co(1)–E(4)	2.282(2)
Ir(1)–E(1)	2.375(2)	Ir(1)–E(2)	2.375(2)
Ir(2)–E(1)	2.367(2)	Ir(2)–E(2)	2.394(2)
Ir(3)–E(3)	2.390(2)	Ir(3)–E(4)	2.373(2)
Ir(4)–E(3)	2.360(2)	Ir(4)–E(4)	2.387(2)
Bond angles			
Ir(1)–Co(1)–Ir(2)	61.54(4)	Co(1)–Ir(1)–Ir(2)	58.51(4)
Co(1)–Ir(2)–Ir(1)	59.95(4)	Ir(3)–Co(1)–Ir(4)	60.89(4)
Co(1)–Ir(3)–Ir(4)	59.03(4)	Co(1)–Ir(4)–Ir(3)	60.09(4)
E(1)–Co(1)–E(2)	96.39(8)	E(1)–Co(1)–E(3)	103.70(9)
E(1)–Co(1)–E(4)	131.1(1)	E(2)–Co(1)–E(3)	129.07(9)
E(2)–Co(1)–E(4)	104.96(9)	E(3)–Co(1)–E(4)	96.09(9)
E(1)–Ir(1)–E(2)	91.39(7)	E(1)–Ir(2)–E(2)	91.13(7)
E(3)–Ir(3)–E(4)	90.73(7)	E(3)–Ir(4)–E(4)	91.33(7)
Co(1)–E(1)–Ir(1)	73.91(7)	Co(1)–E(1)–Ir(2)	72.78(7)
Ir(1)–E(1)–Ir(2)	73.57(6)	Co(1)–E(2)–Ir(1)	73.70(7)
Co(1)–E(2)–Ir(2)	72.07(7)	Ir(1)–E(2)–Ir(2)	73.11(6)
Co(1)–E(3)–Ir(3)	73.82(7)	Co(1)–E(3)–Ir(4)	73.45(7)
Ir(3)–E(3)–Ir(4)	73.00(6)	Co(1)–E(4)–Ir(3)	74.02(7)
Co(1)–E(4)–Ir(4)	72.98(7)	Ir(3)–E(4)–Ir(4)	72.97(6)

Se bond distances in **6** at 2.444(2) and 2.455(2) Å. For comparison, the Pt–Se bond distances in the $Pt(II)_3$ cluster $[\{Pt(PPh_3)_2\}_2\{Pt(cod)\}(\mu_3\text{-}Se)_2][PF_6]_2$ are in the range 2.431(1)–2.474(1) Å [12] and those in the $Pt(II)_2$ complex $[\{Pt(PPh_3)\}_2(\mu_2\text{-}Se)_2]$ are 2.433(1) and 2.465(1) Å [13], all being slightly longer than those in **5**. The Fe–Se bond distances in the selenido clusters containing lower valent Fe centers are e.g. 2.318(3)–2.326(3) Å for $[(Ph_3P)_2N]_2[Fe_3(\mu_3\text{-}Se)(CO)_9]$ [14] and 2.34(2)–2.37(2) Å for $[Fe_3(\mu_3\text{-}Se)_2(CO)_9]$ [15].

In the pentanuclear bow-tie clusters **7** and **8**, the M–Ir distances (M = Fe, Co, Ir) in the range 2.742(2)–2.913(1) Å are all indicative of the presence of metal–metal bonding interactions between these atoms. The Ir–Se bond lengths in these two vary from 2.383(2) to 2.422(2) Å. The Fe–Se bond lengths in **7** from 2.274(3) to 2.282(3) Å are considerably shorter than those in the trinuclear cluster **6**, while the Co–Se bond lengths in $79e^-$ **8** are 2.293(3) and 2.302(3) Å, which are longer only slightly than those in a $78e^-$ cluster **7**. The Co–Se bond lengths reported previously are, for example, 2.332(2)–2.350(2) Å for $[Co_6(\mu_3Se)_8(CO)_6]$ [16] and 2.309(1) and 2.310(1) Å in $[RuCo_2(\mu_3\text{-}Se)(CO)_7(\mu\text{-}Ph_2PCH_2PPh_2)]$ [17]. For comparison, the Fe–S distances in $[(Cp^*Ir)_4Fe(\mu_3\text{-}S)_4][BPh_4]_2$ (**18**) are in the range 2.161(4)–2.171(4) Å and the Co–S distances in $[(Cp^*Ir)_4Co(\mu_3\text{-}S)_4][CoCl_3(MeCN)]_2$ (**19**) are 2.166(6) and 2.183(5) Å with the Ir–S distances from 2.266(3) to 2.298(5) Å [5d]. It is noteworthy that the dihedral angles between two MIr_2 planes differ significantly for M = Fe and Co, the former in **7** being 72.1° with the latter in **8** of 49.0°. This feature was also observed previously for the sulfido analogues, whereby the corresponding dihedral angles were found to be 73.4, 49.9, and 24.3° for **18**, **19** and $[(Cp^*Ir)_4Ni(\mu_3\text{-}S)_4][NiCl_4]\cdot CH_2Cl_2$ [5d], respectively, the former two being in good agreement with those in the Se analogues **6** and **7**. The previous finding for the latter sulfido clusters was able to be interpreted to some extent in terms of the valence electron counts and molecular orbital calculations of these clusters [5d]. However, more recent results on the X-ray analysis of $[(Cp^*Ir)_4Co(\mu_3\text{-}S)_4][BPh_4]_2\cdot CH_2Cl_2$ have implicated that the packing effect exerted by the nature of the anion seems to be the important factor to determine these dihedral angles [18] and further studies are needed to rationalize these findings about the structures of a series of metal–chalcogenido bow-tie clusters of this type.

The structure of μ-selenido–sulfido cluster has been clarified unambiguously for **13**. Thus, the X-ray structure of the cationic cluster **13** has a crystallographically

imposed mirror plane defined by a square planar Pt atom together with the Se, S, P, and Cl atoms, which bisects the Ir–Ir* bond. The Pt–Ir and Ir–Ir* bond distances are 3.041(1) and 2.935(1) Å, respectively. We have previously observed the analogous X-ray structure for the $PdIr_2S_2$ analogue $[(Cp^*Ir)_2\{PdCl(PPh_3)\}(\mu_3\text{-}S)_2]Cl$ (**20**) with the Pd–Ir and Ir–Ir* bond lengths at 3.001(1) and 2.9002(9) [5a]. This core structure of **13** is quite different from that of the neutral $PtIr_2Se_2$ cluster **5**, in which two Pt–Ir distances are apparently unequal with the separations of 2.751(1) and 3.487(1) Å (vide supra). It is to be noted, however, that even for **5**, the ^{1}H-NMR spectrum in $CDCl_3$ at room temperature shows only one singlet due to the Cp* protons, indicating that two Ir centers become equivalent at this temperature in the NMR time scale.

The X-ray structure of **13** clearly shows that the Cl anion trans to the Se atom in **5** is selectively substituted by PPh_3, reflecting the stronger trans effect exerted by Se^{2-} than S^{2-} bound to the Pt(II) center. The Pt–Se bond length at 2.470(1) is longer than those in **5** (2.408(2) and 2.411(2) Å), while the Pt–S distance at 2.350(2) Å is comparable to those in $[(Cp^*Ir)_2\{Pt(dppe)\}(\mu_3\text{-}S)_2][BPh_4]_2$ (2.362(5) and 2.347(4) Å) [5a].

For **14** and **15**, the X-ray analyses have also disclosed the presence of the expected trinuclear and pentanuclear core structures. Thus, the Fe–Ir(1) and Fe–Ir(2) distances in **14** at 2.898(1) and 3.056(1) Å, respectively, are inequivalent. This feature and these distances are analogous to those in the bis(selenido) cluster **6** and the bis(sulfido) cluster **17** shown above. On the other hand, the Co–Ir bond lengths in **15** are in the range 2.755(2)–2.803(2) Å. For comparison, the Co–Ir bond lengths in the bis(selenido) cluster **8** are 2.804(1) and 2.913(1) Å, while those in the bis(sulfido) cluster **19** are 2.746(1) and 2.849(1) Å. The dihedral angle between two $CoIr_2$ planes is 68.2°. In **14** and **15**, since the selenido and sulfido ligands are mutually disordered with the occupancy factor of 0.5, the bonding parameters associated with the chalcogenido ligands are not discussed here.

3. Experimental

3.1. General considerations

All manipulations were carried out under an atomosphere of N_2. IR and NMR spectra were recorded on JASCO FT/IR 420 and JEOL AL-400 spectrometers, respectively. The mass spectra were obtained by a JEOL JMS600H spectrometer. Elemental analyses were performed on a Perkin–Elmer 2400 Series II CHN analyzer. Chemicals were commercially obtained and used as received, while compounds **1a** [3], **9** [19], $[MCl_2(cod)]$ (M = Pd, Pt) [20] were prepared according to the literature methods.

3.2. Preparation of 3

Ethanol (3.0 cm^3) was slowly added to gray Se (80 mg, 1.0 mmol) and $NaBH_4$ (38 mg, 1.0 mmol) at 0 °C and the mixture was stirred for 1 h at room temperature (r.t.). The resultant mixture was dried up in vacuo and to the residue were added a CH_2Cl_2 solution (40 cm^3) of **9** (0.80 g, 1.0 mmol) and then concentrated HCl aq. (120 mg, 1.15 mol) at 0 °C. After stirring for 1 h at this temperature, the resulting solution was dried over $MgSO_4$. The ^{1}H-NMR spectrum of this mixture showed the formation of mono(hydroselenido) complex **10** in 90% yield along with a byproduct **1a** (5%). Unreacted **9** (5%) was also detected. The solution was separated from $MgSO_4$ and then treated with H_2S gas at 0 °C for 5 min. The mixture was evaporated to dryness in vacuo and the residue was washed with acetone and hexane. The yellow solid remained, which contained **3** with a purity of 90% (0.50 g, 60% yield). ^{1}H-NMR (C_6D_6, ppm): isomer **i**, 1.51, 1.30 (s, 15H each, Cp*), 1.12 (s, 1H, SH), –2.47 (s, 1H, SeH); isomer **ii**, 1.43, 1.39 (s, 15H each, Cp*), 1.23 (s, 1H, SH), −2.37 (s, 1H, SeH); the ratio of isomers **i** and **ii** is 3:2. Two isomers **i** and **ii** may be assigned as *syn* and *anti* forms, respectively (see text).

3.3. Preparation of 4

A solution containing **1a** (0.44 g, 0.50 mmol) and $[PdCl_2(cod)]$ (0.14 g, 0.50 mmol) in THF (10 cm^3) was stirred at r.t. for 5 h. The green suspension was evaporated to dryness in vacuo and the residue was extracted with CH_2Cl_2. Addition of ether to the concentrated extract afforded **4** as green crystals (0.44g, 89% yield). Anal. Calc. for $C_{20}H_{30}Cl_2Ir_2PdSe_2$: C, 24.26; H, 3.05. Found: C, 24.44; H, 3.25%. ^{1}H-NMR ($CDCl_3$, ppm): 2.10 (s, Cp*).

3.4. Preparation of 5

This complex was obtained from **1a** (0.45 g, 0.50 mmol) and $[PtCl_2(cod)]$ (0.19 g, 0.50 mmol) by the same method as that for **4** as green crystals in 46% yield (0.25 g). Anal. Calc. for $C_{20}H_{30}Cl_2Ir_2PtSe_2$: C, 22.27; H, 2.80. Found: C, 22.16; H, 3.00%. ^{1}H-NMR ($CDCl_3$, ppm): 2.10 (s, Cp*). Single crystals of $\mathbf{5}\cdot 1/2ClCH_2CH_2Cl$ for the X-ray diffraction were available by recrystallization from $ClCH_2CH_2Cl$–ether.

3.5. Preparation of 6

This complex was obtained as black crystals in 54% yield (50 mg) from **1a** (87 mg, 0.098 mmol) and $FeCl_2$ (13 mg, 0.10 mmol) in THF (3 cm^3) by the same method

as that for **4** except that the evaporated reaction mixture residue was crystallized from CH_2Cl_2–hexane. Anal. Calc. for $C_{20}H_{30}Cl_2Ir_2FeSe_2$: C, 25.57; H, 3.22. Found: C, 25.55; H, 3.19%.

3.6. Preparation of 7

(1) Into a suspension of **6** (66 mg, 0.070 mmol) and **1a** (62 mg, 0.070 mmol) in THF (5 cm^3) was added $NaBPh_4$ (96 mg, 0.28 mmol) and the mixture was stirred at r.t. for 6 h. The resultant mixture was dried up in vacuo and the residue was extracted with CH_2Cl_2. Addition of ether to the concentrated extract gave **7**·CH_2Cl_2 as red crystals (140 mg, 83%). Anal. Calc. for $C_{89}H_{102}B_2Cl_2FeIr_4Se_4$: C, 44.45; H, 4.28. Found: C, 44.53; H, 4.20%. ^{1}H-NMR (CD_2Cl_2, ppm): 1.92 (s, 60H, Cp*), 6.87 (t, 8H, *p*-H of BPh), 7.02 (t, 16H, *m*-H of BPh), 7.29 (m, 16H, *o*-H of BPh). The presence of the solvating CH_2Cl_2 was confirmed by recording ^{1}H-NMR spectrum in $CDCl_3$. On the other hand, the single crystal used for the X-ray diffraction study did not contain CH_2Cl_2.

(2) Into a suspension of **6** (57 mg, 0.061 mmol) in THF (5 cm^3) was added $NaBPh_4$ (83 mg, 0.24 mmol) and the mixture was treated analogously. The yield of **7**·CH_2Cl_2 was 51 mg (70% based on Ir atom).

3.7. Preparation of 8

A suspension containing **1a** (0.18 g, 0.20 mmol) and $CoCl_2$ (39 mg, 0.30 mmol) in THF (7 cm^3) was stirred at r.t. for 1 day. The resultant mixture was filtered off and the black solid remained was extracted with MeCN. Addition of hexane to the concentrated extract afforded black crystals of **8** (0.14 g, 68%). Anal. Calc. for $C_{44}H_{66}N_2Cl_6Co_3Ir_4Se_4$: C, 25.20; H, 3.17. Found: C, 25.25; H, 3.20%.

3.8. Preparation of 11

This cluster was prepared from **3** (0.17 g,0.20 mmol) and [$PdCl_2$(cod)] (57 mg, 0.20 mmol) as described for preparing **4**. Green crystals (0.13 g, 69% yield). Anal. Calc. for $C_{20}H_{30}Cl_2Ir_2PdSSe$: C, 25.47; H, 3.21. Found: C, 25.83; H, 3.31%. ^{1}H-NMR ($CDCl_3$, ppm): 2.12 (s, Cp*).

3.9. Preparation of 12

This cluster was obtained from **3** (0.17 g, 0.20 mmol) and [$PtCl_2$(cod)] (78 mg, 0.21 mmol) similarly. Green crystals (0.12 g, 58% yield). Anal. Calc. for $C_{20}H_{30}Cl_2Ir_2PtSSe$: C, 23.28; H, 2.93. Found: C, 23.06; H, 2.89%. ^{1}H-NMR ($CDCl_3$, ppm): 2.12 (s, Cp*).

3.10. Preparation of 13

Into a solution of **12** (47 mg, 0.046 mmol) in CH_2Cl_2 (5 cm^3) was added PPh_3 (12 mg, 0.046 mmol) and the mixture was stirred for 1 day at r.t. The resultant mixture was dried up in vacuo, and the residue was washed with ether and then extracted with CH_2Cl_2. Addition of hexane to the concentrated extract afforded **13**·CH_2Cl_2 as green crystals (39 mg, 66% yield). Anal. Calc. for $C_{39}H_{47}Cl_4Ir_2PPtSSe$: C, 33.97; H, 3.43. Found: C, 34.27; H, 3.56%. ^{1}H-NMR ($CDCl_3$, ppm): 2.07 (s, Cp*), 5.29 (s, 2H, CH_2Cl_2), 7.16 (t, 6H, *o*-H of PPh_3), 7.36 (t, 6H, *m*-H of PPh_3), 7.48 (m, 3H, *p*-H of PPh_3). ^{31}P-NMR ($CDCl_3$, ppm): −0.71 (s).

3.11. Preparation of 14

This complex was prepared from **3** (0.23 g, 0.27 mmol) and $FeCl_2$ (35 mg, 0.28 mmol) by an analogous method to that for **6**. Black crystals (0.14 g, 58% yield). Anal. Calc. for $C_{20}H_{30}Cl_2FeIr_2SSe$: C, 26.91; H, 3.39; S, 3.59. Found: C, 26.66; H, 3.29; S, 3.24%. FABMS *m*/*z* 857 ([**14**−Cl]$^+$).

3.12. Preparation of 15

This cluster was obtained as **15**·CH_2Cl_2 from the reaction of **3** (0.17 g, 0.20 mmol) and $CoCl_2$ (40 mg, 0.30 mmol) carried out similarly to that for preparing **8**. Black crystals (79 mg, 39% yield). Anal. Calc. for $C_{44}H_{66}N_2Cl_6Co_3Ir_4S_2Se_2$: C, 26.38; H, 3.32; N, 1.40. Found: C, 26.18; H, 3.29; N, 1.50%.

3.13. Preparation of 16

Into a suspension of **14** (0.10 g, 0.11 mmol) and **3** (0.094 g, 0.11 mmol) in THF (8 cm^3) was added $NaBPh_4$ (0.15 g, 0.44 mmol) and the mixture was stirred for 1 day. The resultant mixture was filtered off and the remained solid was extracted with CH_2Cl_2. Addition of hexane to the concentrated extract afforded the red crystals of **16**·CH_2Cl_2 (0.13 g, 50% yield). Anal. Calc. for $C_{89}H_{102}B_2Cl_2FeIr_4S_2Se_2$: C, 46.25; H, 4.45. Found: C, 46.63; H, 4.61%. ^{1}H-NMR (CD_2Cl_2, ppm): 2.24 (s, 60H, Cp*), 6.87 (t, 8H, *p*-H of BPh), 7.02 (t, 16H, *m*-H of BPh), 7.31 (m, 16H, *o*-H of BPh). The presence of the solvating CH_2Cl_2 was confirmed by recording ^{1}H-NMR spectrum in $CDCl_3$.

3.14. X-ray diffraction studies

The X-ray analyses of **5**·1/2$ClCH_2CH_2Cl$, **6**, **7**, **8**, **13**·CH_2Cl_2, **14**, and **15**·CH_2Cl_2 were carried out at r.t. on a Rigaku AFC7R diffractometer equipped with a graphite-monocromatized Mo–K_α source. Intensity data were corrected for the Lorentz-polarization effect and

Table 8
Crystallographic data for **5**·1/2ClCH$_2$CH$_2$Cl, **6**, **7**, **8**, **13**·CH$_2$Cl$_2$, **14** and **15**·CH$_2$Cl$_2$

	5·1/2ClCH$_2$CH$_2$Cl	**6**	**7**	**8**	**13**·CH$_2$Cl$_2$	**14**	**15**·CH$_2$Cl$_2$
Formula	$C_{21}H_{32}Cl_3Ir_2PtSe_2$	$C_{20}H_{30}Cl_2FeIr_2Se_2$	$C_{90}H_{103}NB_2FeIr_4Se_4$	$C_{44}H_{66}N_2Cl_6Co_3Ir_4Se_4$	$C_{39}H_{47}Cl_4Ir_2PPtSSe$	$C_{20}H_{30}Cl_2FeIr_2SeS$	$C_{89}H_{102}B_2Cl_2CoIr_4Se_2S_2$
Formula weight	1128.29	939.57	2361.00	2097.26	1379.14	892.67	2314.16
Space group	*Pbca* (no. 61)	*C*2/*c* (no. 15)	$P\bar{1}$ (no. 2)	*C*2/*c* (no. 15)	$P2_1/m$ (no. 11)	*C*2/*c* (no. 15)	$P\bar{1}$ (no. 2)
Unit cell dimensions							
a (Å)	20.265(5)	33.989(4)	11.391(5)	29.125(4)	14.635(2)	33.725(5)	11.935(2)
b (Å)	16.513(1)	8.919(2)	16.92(1)	8.608(2)	12.635(1)	8.871(2)	16.937(2)
c (Å)	16.375(2)	17.564(2)	23.61(1)	23.951(1)	11.956(1)	17.505(3)	23.752(8)
α (°)	90.00	90.00	76.18(5)	90.00	90.00	90.00	75.98(2)
β (°)	90.00	109.96(1)	77.54(5)	98.18(1)	93.013(8)	109.77(1)	78.32(2)
γ (°)	90.00	90.00	78.29(8)	90.00	90.00	90.00	77.99(1)
V (Å^3)	5479(1)	5004(1)	4258(4)	5943(1)	2207.8(4)	4928.1(1)	4304.5(2)
Z	8	8	2	4	2	8	2
ρ_{calc} (g cm^{-3})	2.735	2.494	1.841	2.344	2.074	2.406	1.785
μ_{calc} (cm^{-1})	177.47	143.39	81.64	125.11	103.53	131.68	73.65
Crystal size (mm^3)	0.50 × 0.20 × 0.10	0.40 × 0.20 × 0.10	0.40 × 0.20 × 0.15	0.40 × 0.20 × 0.10	0.40 × 0.30 × 0.20	0.30 × 0.25 × 0.20	0.40 × 0.20 × 0.20
Number of data	3610 ($I > 3.00\sigma(I)$)	3737 ($I > 3.00\sigma(I)$)	7240 ($I > 3.00\sigma(I)$)	3465 ($I > 3.00\sigma(I)$)	4056 ($I > 3.00\sigma(I)$)	4345 ($I > 3.00\sigma(I)$)	10815 ($I > 3.00\sigma(I)$)
Number of variables	262	245	919	285	265	275	1022
Transmission factor	0.1345–0.9991	0.2609–0.9992	0.5026–0.9968	0.0813–0.9976	0.5935–0.9995	0.6339–0.9995	0.7569–0.9988
R [a]	0.049	0.037	0.076	0.063	0.039	0.031	0.048
R_w [b] or wR_2 [c]	0.050 [b]	0.039 [b]	0.117 [b]	0.065 [b]	0.102 [c]	0.087 [c]	0.114 [c]
GOF [d]	1.71	1.34	1.68	1.81	1.01	0.99	1.09
Residual peaks (e$^-$ Å^{-3})	2.58, −1.80	1.48, −1.38	1.95, −1.90	3.71, −3.31	2.69, −2.00	1.22, −1.58	1.58, −1.69

[a] $R = \Sigma||F_o| - |F_c||/\Sigma|F_o|$.
[b] $R_w = [\Sigma\ w(|F_o| - |F_c|)^2/\Sigma\ wF_o^2]^{1/2}$ ($w = [\{\sigma(F_o)\}^2 + (p^2/4)F_o^2]^{-1}$).
[c] $wR_2 = [\Sigma\ w(F_o^2 - F_c^2)^2/\Sigma\ w(F_o^2)^2]^{1/2}$.
[d] GOF $= [\Sigma\ w(|F_o| - |F_c|)^2/\{(\text{no. observed}) - (\text{no. variables})\}]^{1/2}$.

for absorption (ψ-scans). Details of crystal and data collection parameters are listed in Table 8.

Structure solution and refinements were conducted by using the TEXSAN program package [21]. The positions of non-hydrogen atoms were determined by DIRDIF PATTY [22] and were refined anisotropically. Hydrogen atoms were placed at ideal positions and included at the final stages of refinements with fixed parameters. For **5**·1/2$ClCH_2CH_2Cl$, half of the solvating dichloroethane molecule is independent, in which the C(21) atom is disordered over two positions with same occupancies. Hydrogen atoms attached to C(21) were not included in the refinements. In **14** and **15**·CH_2Cl_2, the positions of bridging chalcogenido atoms were occupied by the Se and S atoms with the same occupancies. These atoms denoted as E in Figs. 6 and 7 as well as Tables 6 and 7 were refined, assuming the occupancies of 0.735 by only Se.

4. Supplementary material

Crystallographic data for the structural analysis have been deposited with the Cambridge Crystallographic Data Centre, CCDC nos. 201924–201930 for compounds **6**, **5**, **7**, **8**, **14**, **13**, and **15**, respectively. Copies of this information may be obtained free of charge from The Director, CCDC, 12 Union Road, Cambridge CB2 1EZ, UK (Fax: +44-1223-336033; e-mail: deposit@ccdc.cam.ac.uk or www: http://www.ccdc.cam.ac.uk).

Acknowledgements

Financial support by the JSPS FY 2001 'Research for the Future Program' and the Grant in Aid for Scientific Research from the Ministry of Education, Science, Sports, and Culture of Japan (No. 14078206) is appreciated.

References

[1] (a) M. Hidai, S. Kuwata, Y. Mizobe, Acc. Chem. Res. 33 (2000) 46;
(b) T. Masumori, H. Seino, Y. Mizobe, M. Hidai, Inorg. Chem. 39 (2000) 5002;
(c) S. Kabashima, S. Kuwata, K. Ueno, M. Shiro, M. Hidai, Angew. Chem. Int. Ed. Engl. 39 (2000) 1128;
(d) S. Kuwata, S. Kabashima, Y. Ishii, M. Hidai, J. Am. Chem. Soc. 123 (2001) 3826;
(e) S. Kuwata, S. Kabashima, N. Sugiyama, Y. Ishii, M. Hidai, Inorg. Chem. 40 (2001) 2034;
(f) F. Takagi, H. Seino, Y. Mizobe, M. Hidai, Organometallics 21 (2002) 694 (and references therein).
[2] (a) S. Nagao, H. Seino, Y. Mizobe, M. Hidai, Chem. Commun. (2000) 207;
(b) S. Nagao, H. Seino, T. Okada, Y. Mizobe, M. Hidai, J. Chem. Soc. Dalton Trans. (2000) 3546.
[3] H. Seino, Y. Mizobe, M. Hidai, Organometallics 19 (2000) 3631.
[4] H. Seino, Y. Mizobe, M. Hidai, New J. Chem. 24 (2000) 907.
[5] (a) D. Masui, T. Kochi, Z. Tang, Y. Ishii, Y. Mizobe, M. Hidai, J. Organomet. Chem. 620 (2001) 69;
(b) T. Kochi, Y. Nomura, Z. Tang, Y. Ishii, Y.Mizobe, M. Hidai, J. Chem. Soc. Dalton Trans. (1999) 2575;
(c) Z. Tang, Y. Nomura, Y. Ishii, Y. Mizobe, M. Hidai, Organometallics 16 (1997) 151;
(d) Z. Tang, Y. Nomura, S. Kuwata, Y. Ishi, Y. Mizobe, M. Hidai, Inorg. Chem. 37 (1998) 4909;
(e) S. Kuwata, M. Andou, K. Hashizume, Y. Mizobe, M. Hidai, Organometallics 17 (1998) 3429;
(f) K. Hashizume, Y. Mizobe, M. Hidai, Organometallics 15 (1996) 3303.
[6] Z. Tang, Y. Nomura, Y. Ishii, Y. Mizobe, M. Hidai, Inorg. Chim. Acta 267 (1998) 73.
[7] (a) P. Mathur, P. Payra, S. Ghose, Md.M. Hossain, C.V.V. Satyanarayana, F.O. Chicote, P.K. Chadha, J. Organomet. Chem. 606 (2000) 176;
(b) P. Mathur, S. Chatterjee, S. Ghose, M.F. Mahon, J. Organomet. Chem. 587 (1999) 93 (and references therein).
[8] H. Seino, M. Hidai, Y. Mizobe, Chem. Lett. (2002) 920.
[9] D. Cauzzi, C. Graiff, C. Massera, G. Predieri, A. Tipicchio, D. Acquotti, J. Chem. Soc. Dalton Trans. (1999) 3515.
[10] J.A. Dean (Ed.), Lange's Handbook of Chemistry, Tables 3–10, McGraw Hill, New York, 1985.
[11] S. Schulz, M. Andruh, T. Pape, T. Heinze, H.W. Roesky, L. Häming, A. Kuhn, R. Herbst-Irmer, Organometallics 13 (1994) 4004.
[12] J.S.L. Yeo, J.J. Vittal, W. Henderson, T.S.A. Hor, Inorg. Chem. 41 (2002) 1194.
[13] A. Bencini, M.D. Vaira, R. Morassi, P. Stoppioni, F. Mele, Polyhedron 15 (1996) 2079.
[14] R.E. Bachman, K.H. Whitmire, Inorg. Chem. 33 (1994) 2527.
[15] L.F. Dahl, P.W. Sutton, Inorg. Chem. 2 (1963) 1067.
[16] G. Gervasio, S.F.A. Kettle, F. Musso, R. Rossetti, P.L. Stanghellini, Inorg. Chem. 34 (1995) 298.
[17] P. Braunstein, C. Graiff, C. Massera, G. Predieri, J. Rosé, A. Tiripicchio, Inorg. Chem. 41 (2002) 1372.
[18] M. Iwasaki, Private communication (2001).
[19] R.N. Grimes, Inorg. Synth. 29 (1992) 229.
[20] D. Drew, J.R. Doyle, Inorg. Synth. 28 (1990) 346.
[21] TEXSAN: Crystal Structure Analysis Package, Molecular Structure Corp., The Woodlands, TX, 1985 and 1992.
[22] P.T. Beurskens, G. Admiraal, G. Beurskens, W.P. Bosman, S. Garcia-Granda, R.O. Gould, J.M.M. Smits, C. Amykall, PATTY: The DIRDIF Program System, Technical Report of the Crystallography Laboratory, University of Nijmegen, The Netherlands, 1992.